



PERFORMANCE ANALYSIS OF A SMALL-SCALE GRID-CONNECTED PHOTOVOLTAIC SYSTEM: A REAL CASE STUDY IN EGYPT

Hossam Abobakr^{*1}, Ahmed A. Zaki Diab^{2,*}, Yahia B. Hassan³, and Ashraf A. M. Khalaf⁴

^{1,2,4}Electrical Engineering Department, Faculty of Engineering, Minia 61111, Egypt

³Higher Institute of Engineering, Minia 61111, Egypt

*Corresponding Author E-mail: enghossam841@gmail.com

ABSTRACT:

Renewable energy sources, especially PV systems, which become more significant sources of energy, are attracting considerable commercial interest. Nonetheless, the integration of the PV power plants to the utility grids may cause several operational problems for distribution networks. The severity of these problems directly depends on the percentage of PV penetration and the geography of the installation. Hence, knowing the possible impact of small grid-connected PV systems on distribution networks can provide feasible solutions before practical implementations in real-time. The electrical power generated from photovoltaic (PV) array depends mainly on the weather conditions. So, the PV solar grid-connected inverters should equip with the control system to meet a fast response of solar irradiance change. This study includes performance analysis for data and measurements which real-time from the PV grid-connected system site according to Egyptian PV-LV code-2014, simulation by using MATLAB/Simulink, and cost analysis for connecting small-scale 39.78 kW photovoltaic (SSPV) system to LV distribution networks. Power quality parameters are measured for the output of the installed PV system at the Holy Family School in Helwan, Egypt. The proposed system model is built on MATLAB/Simulink and simulated under daily weather conditions to test its operating performance. The power quality indices at the inverter output side have been measured using PA-9-plus power quality analyzer. The cost analysis of SSPV generator based on the weather conditions will lead to new investments. The system has been installed in October 2016, produces 68.966MWh/year annual energy yield, and reaches its initial cost in 6.2198 years. The produced electricity by the system is injected directly into the grid without storage devices (On-grid Plant).

Keywords: *Photovoltaic system, Grid-connected, Power quality, Egyptian PV-LV code, Simulation, Cost analysis, Case study*

1. INTRODUCTION

Renewable energy sources are used to improve the quality of power sources due to global warming and environmental conditions [1]. Moreover, variations in solar irradiation can cause power fluctuation and voltage flicker, resulting in undesirable effects on high penetrated PV systems in the power system [2]. The efficient and proper

operation of photovoltaic systems are dependent on the fluctuation of solar irradiance; temperature and choice of power semiconductor devices are some of the parameters that affect the power quality of the grid-connected PV systems. Good power quality translates into obtaining a sinusoidal voltage and current output from the photovoltaic system; in order to avoid harmonics and eventually voltage distortion [3].

Economic incentives, reduction in cost, and the fast-technological developments allow the use of grid-connected PV plants in a simple, efficient and profitable way [4].

This paper specifies the performance analysis by recording measurements, simulation and cost analysis for connecting 39.78 kW PV system to low voltage (LV) distribution network. It presents and evaluate the measurements based on power quality quantities which are obtained from the PV grid-connected system site and the

MATLAB SIMULINK simulation. Power quality parameters (active power, reactive power, power factor, voltage, flicker, and total harmonic distortion) are measured from the output of the installed PV system over a period of three days at the considered set. The power quality of provided by the SSPV systems is governed by Egyptian standard (PV-LV code-2014) on voltage, flicker, frequency, harmonics and power factor (PF) at the point of common coupling (PCC).

The paper investigates the various effects for connecting SSPV systems to LV distribution networks by measuring PV array output, AC Side results and THD parameters for the output of the simulated PV system at the MATLAB SIMULINK. The paper discusses the cost analysis and breakeven point of SSPV system.

2. GRID-CONNECTED PV SYSTEM DESCRIPTION

2.1. System Overview

A 39.78 kW peak (kWp) small-scale grid-connected PV system was installed at the Holy Family School in Helwan, Egypt as shown in Fig. 1. The main components of a SSPV power plant are PV modules, mounting (or tracking) systems, inverters, and the grid connection. The considered system consists of 3 main parts that are solar PV array, grid-connected inverter, and monitoring system. Table 1 shows the system overview.



Fig. 1. Photo of the PV array on the School rooftop.

THE PROJECT INFORMATION

Longitude	29° 50' 48.52	Latitude	31° 19' 58.62
Interconnection voltage	380V/220V	Meter type	Feeding tariff
Peak power	39.78 kW	Annual Energy	68,627 kWh
Tilt angle	30°	Mounting structure	Fixed
Module model	Suntech Power STP255-20/Wd	Inverter model	Sunny Tripower STP 20000TL-30
No. of modules	156	No. of Inverters	2
No. of strings	8	No. of modules per strings	20/4 + 19/4

2.2. PV Modules

The grid-connected PV system includes 156 multi-crystalline modules covering a total area of 400 m². The electrical characteristics of each PV module are summarized in Table 2

PV MODULE ELECTRICAL CHARACTERISTICS AT STANDARD TEST CONDITION (STC).

STC	STP255-20/wd
Maximum Power at STC (P _{max})	255 W
Maximum Operating Voltage (V _{mp})	30.8 V
Maximum Operating Current (I _{mp})	8.28 A
Open Circuit Voltage (V _{oc})	37.6 V
Short Circuit Current (I _{sc})	8.76 A
Module Efficiency	15.7%

2.3. Grid-Connected Inverter

The output terminals of the solar PV array are connected to a Sunny Tri power

20000TL 3ph grid-connected inverter. This inverter is turned-on all-day time and automatically synchronizes to the electric grid. If the electric grid has a problem like shutdown or unusual problems, the inverter stops its operation for operator safety. Table 3 shows the Sunny Tri power 20000TL 3ph grid-connected inverter parameters. The electrical data are measured by the measurement function of the inverter. This inverter shows on its screen the PV system power transmitted to the electric grid, system voltage and amount of produced energy during the day and total runtime, etc.

Since the array voltage and current vary considerably depending upon the weather conditions, the inverter needs to move its working point to function optimally. To feed the maximum power into the electricity grid, the inverter must work at the maximum power point (MPP) of the PV array. The MPP tracker ensures that the inverter is adjusted to the MPP point and the great test possible power is fed into the mains electricity grid.

The efficiency of the solar inverter can be defined based on the values of electrical DC power delivered to the inverter from PV panels (P_{DC}) and the AC power obtained from the inverter (P_{AC}). The instantaneous inverter efficiency (η_{inv}) is defined as the ratio of output to input power:

$$\eta_{inv} = \frac{P_{AC}}{P_{DC}} \quad (1)$$

The PV array efficiency (η_{PV}) is calculated as:

$$\eta_{PV} = \frac{P_{DC}}{G \times A} \quad (2)$$

Where A is the total active area of PV array, m^2 .

G is the total in-plane irradiance, kw/m^2 .

The instantaneous reference yield (y_r), which is the ratio of the total irradiance ($G(kW/m^2)$) to the reference irradiance ($G_{stc} = 1kW/m^2$), is given by

$$y_r = \frac{G}{G_{stc}} \quad (3)$$

While the instantaneous array yield (y_A), which is the ratio of the PV array output power (P_{DC}) to the peak power ($P_{max,stc}$) of the installed PV array.

$$y_A = \frac{P_{DC}}{P_{max,stc}} \quad (4)$$

The instantaneous (y_f) can be calculated as follows:

$$y_f = \frac{P_{AC}}{P_{max,stc}} \quad (5)$$

The performance ratio is used to assess the quality of PV installation which is widely reported on a daily, monthly and yearly basis. The instantaneous performance ratio (p_r), is expressed in percentage to describe the overall losses of the PV system output and can be defined by the following equations:

$$P_r = \frac{y_f}{y_r} \quad (6)$$

GRID-CONNECTED INVERTER PARAMETERS

Input (DC)	
Max. array power	30000 W _p STC
Max. DC voltage	1000 V
MPPT operating voltage range	150 V...1000 V
Min. DC voltage / start voltage	150 V / 188 V
Number of MPP tracker inputs	2
Max. operating input- current / per MPP tracker	66 A / 33 A
Max. short circuit current per MPPT / string input	53 A / 53 A
Output (AC)	
AC nominal power	20000 W
Max. AC apparent power	20000 VA
Output phases / line connections	3 / 3-N-PE
Nominal AC voltage	480 / 277 V WYE
AC voltage range	244 V...305 V
Rated AC grid frequency	50 Hz
AC grid frequency / range	50 HZ, 60 HZ / -6 HZ...+5 HZ
Max. output current	24 A
Power factor at rated power / adjustable displacement	1 / 0.0 leading...lagging
Harmonics	< 3%

2.4. Monitoring and Data Acquisition System

Figure 2 shows a photo for the used monitoring and data acquisition system. The figure shows PA-9 plus power quality analyzer was connected to the output of PV power plants at PCC. All real-time electrical data are logged into this monitoring system. PA-9 plus power quality analyzer Trends voltage, current, imbalance, power, energy, events, flicker (PST/PLT), THD, TDD, individual harmonics, and frequency according to standards (EN50160, IEC61000-4-15, IEEE1159/519)

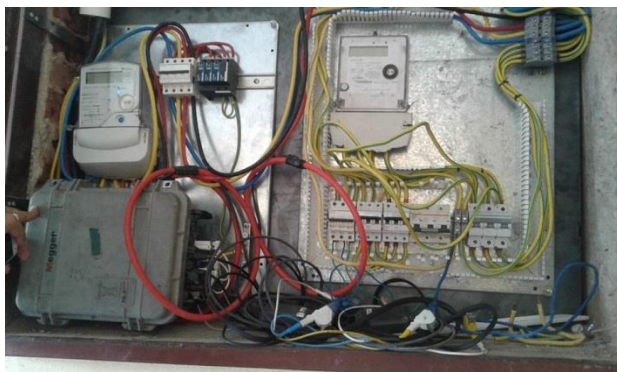


Fig.2. Photo of PA-9 plus Power Analyzer.

2.5. Single Line Diagram (SLD)

The PV array is divided into four strings. Moreover, each string is connected through an inverter with an average PV output voltage 600V. Two strings are built from interconnecting of 20 panels in series connected to input A and two strings are built from interconnecting 19 panels in series connected to input B for each inverter. The system overview is shown in Table 4.

The outputs of the strings are pooled in the array combiner box through DC fuses. A surge protector is incorporated in the system for transient protection and as a DC disconnect switch. The output of the array is brought to the control room, where the DC power is fed to the power conditioning unit.

20 kW Sunny Tri power inverter, that includes filters, maximum power point tracking and control unit, is used to convert the DC PV power into AC power (three phase-four wire), 380V, 50 Hz and to synchronize it with the utility grid (UG). The output of the inverter can follow the grid voltage, frequency, phase sequence, and phase shift during its normal operation. A single line diagram of the set-up grid-connected system is shown in Fig. 3 which show the PV power quality monitoring system is set around PA-9 plus power quality analyzer.

GRID-CONNECTED INVERTER PARAMETERS

<i>PV design data</i>	<i>Input A</i>	<i>Input B</i>
Suntech Power STP255-20/Wd	40	38
Azimuth / Tilt angle	0° / 30°	0° / 30°
Number of Strings	2	2
PV modules per string	20	19
Peak power input	10.2 kWp	9.69kWp
Typical PV Voltage	539 V	512 V
Min. PV Voltage	502 V	477 V
Min. DC Voltage	150 V	150 V
Max. PV voltage	797 V	758 V
Max. DC voltage	1000 V	1000 V
Max. current	16.5 A	16.5 A
Max. DC current	33 A	33 A

This analyzer is designed as a universal meter for the entire field of power electronics and network analysis. It can be used practically in all power electronics applications, systems testing, and quality assurance. It can be used for measurements in motors, transformers, conventional and switched power supply units. The monitored results are collected using 1 s step. The recorded data are exported and averaged every 10 min and stored on the hard disk for analysis and evaluation.

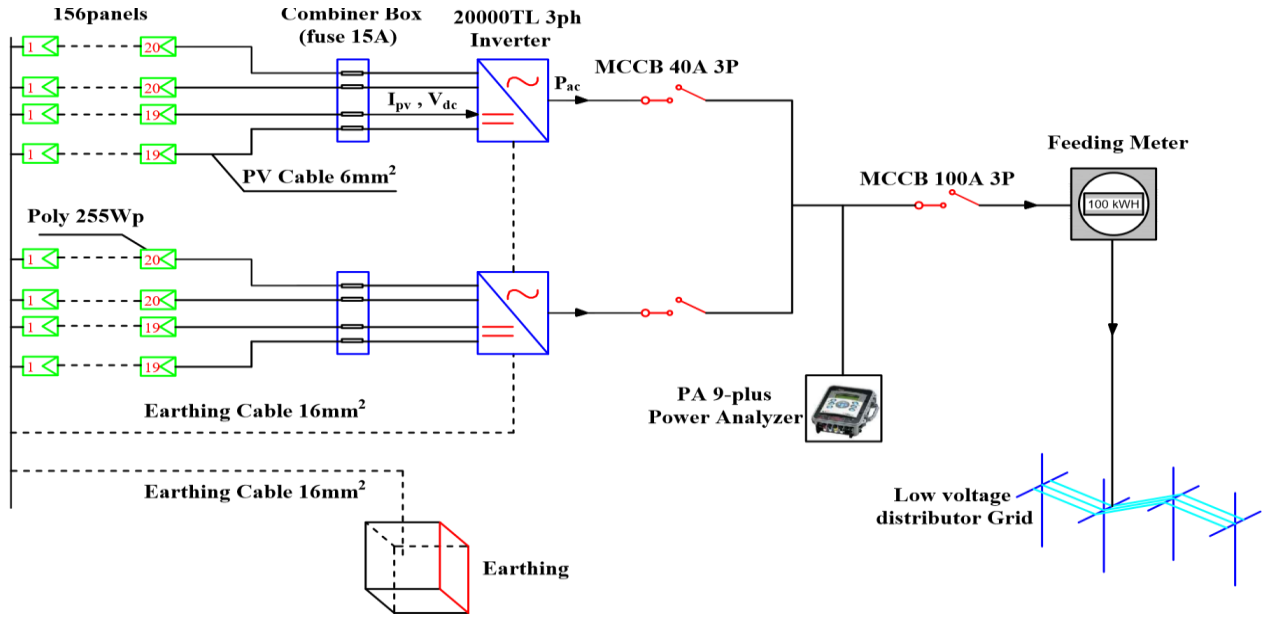


Fig.3. The single line diagram (SLD) of the SSPV.

3. SYSTEM MODELLING

The MATLAB SIMULINK model consists of 156 PV arrays of solar panel STP255-20/wed, the DC-DC boost converter for boosting the PV voltage to a level that is adequate for the inverter to produce a maximum output voltage, a three-phase VSI connected between DC link capacitor (i.e. acts as a temporary power storage device to provide the VSI with a steady flow of power) and LC filter to prevent harmonics from propagating into the UG. The normal PV voltage is 290 Vdc at a solar irradiance of 1000 W/m², which sets up to 500 Vdc via DC-DC boost converter and then converted into AC voltage by a three-level VSI up to 20 kV through a step-up transformer to inject to the grid.

3.1. Modeling of PV ARRAY

The modules of PV array are connected in series and parallel manner to give rated power. The 'Module' parameter of the PV Array block allows you to choose among various array types of the NREL System Advisor Model.

The manufacturer specifications for one module are:

- Number of cells per module: $N_{cell} = 60$
- Open-circuit voltage: $V_{OC} = 37.5$ V

- Short-circuit current: $I_{SC} = 8.73$ A
- Voltage and current at maximum power: $V_{mp} = 30.9$ V, $I_{mp} = 8.26$ A

Figure 4 illustrates the electrical circuit of the PV array based on accurate two diode model $R_s(N_s/N_p)$.

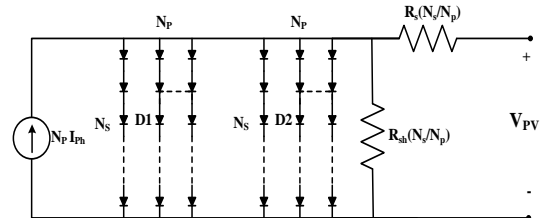


Fig. 4. The equivalent circuit of the single diode model for PV array.

The output current (I_{PV}) of the PV array is given by[5]:

$$I_{PV} = N_p I_{ph} - N_p I_{s1} \left[\exp \left(\frac{1}{a_1 V_T} \left(\frac{V_{PV}}{N_s} + \frac{I_{PV} R_s}{N_s} \right) \right) - 1 \right] - N_p I_{s2} \left[\exp \left(\frac{1}{a_2 V_T} \left(\frac{V_{PV}}{N_s} + \frac{I_{PV} R_s}{N_s} \right) \right) - 1 \right] - \frac{1}{R_{sh}} \left(\frac{V_{PV}}{N_s} + \frac{I_{PV} R_s}{N_s} \right) \quad (7)$$

where:

I_{s1} is the saturation current of diode D_1 .

I_{s2} is the saturation current of diode D_2

V_T is the thermal voltage ($V_T = Ns \frac{KT}{q}$)

k is the Boltzmann constant,

T is the absolute temperature in degrees Kelvin

q is the electronic charge ($1.6 * 10^{-19}$ C)

a_1 is idealist factor of diode D_1

a_2 is idealist factor of diode D_2

V_{PV} is the output voltage of the PV array

R_s , and R_{sh} are series and shunt resistances of PV cells

N_s and N_p are the number of series and parallel cells, respectively I_{ph}

3.2.. Modeling of DC-DC Boost Converter

Figure 5 shows the configuration of the DC-DC boost converter. Moreover, output and input relations of the DC-DC boost converter during continues mode operation are given as follows [6-8]:

$$V_{DC} = \frac{V_{PV}}{1-D} \quad (8)$$

$$L_{boost} = \frac{V_{PV}(V_{DC}-V_{PV})}{\Delta i_{Lboost} f_s V_{DC}} \quad (9)$$

$$C_B = \frac{\Delta i_L}{8 f_s \Delta V_{PV}} \quad (10)$$

$$C_{DC} = \frac{P_{PV}}{2.0 w_g V_{DC} \Delta V_{DC}} \quad (11)$$

Where:

Δi_{Lboost} is the amplitude of ripple boost inductor current 1.4 %,

f_s is the switching frequency of the boost converter power switch.

V_{DC} is the main voltage across the DC capacitor = 500V.

ΔV_{PV} is the amplitude of ripple PV output voltage = 0.4%.

P_{PV} is the rated power of PV system = 100 kW.

w_g is the utility grid angular frequency in rad/sec = 314.0 rad/s.

ΔV_{DC} is the amplitude of ripple capacitor voltage =10%.,

The DC-DC boost converter parameters are computed

from Eqs. (8:11).

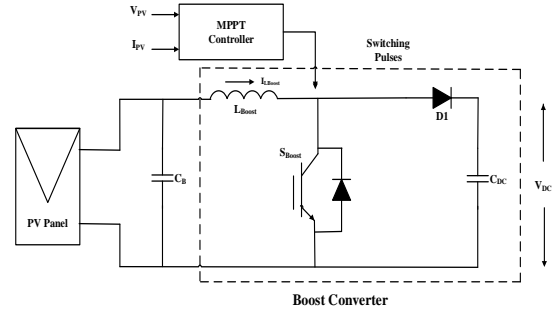


Fig.5. DC-DC boost converter with its controller.

3.2.1. Power Filter

The UG interface contains filters to reduce the harmonics generated by the inverter and to neutralize spikes coming from the UG [9]. Figure 6 shows the model of power filter considered in this system. The filter is a three-phase passive filter of second-order low pass filter and installed at the output of three phases VSI.

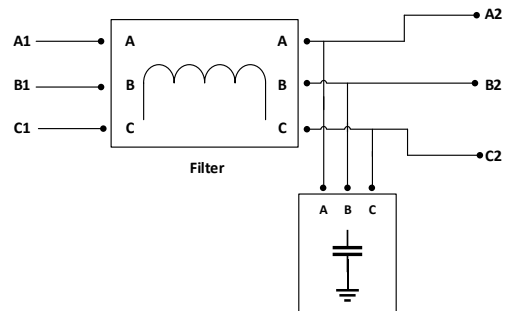


Fig.6. LC power filter model connected at the output of PV inverter.

The selection of the capacitor is a trade-off between reactive power supplied by the capacitor at the fundamental frequency and coil inductance. The increasing capacitance value will reduce the efficiency of the inverter while reducing the capacitance value of LC filter will increase the inductor and its voltage drop across the network. Normally the reactive power of the capacitor is

suggested less than 15% of the rated inverter power. In such a design, the reactive power is chosen as 10% of the rated power of the inverter [10].

$$C_f = 10\% (P_{PV} / (3 * 2\pi f_g V_g^2)) \quad (12)$$

The selection of filter inductance L_f depends on the resonance frequency of the filter that is should be greater than or equal to 10th of the grid frequency to avoid resonance with the grid network. So, the filter inductance is expressed as:

$$L_f \leq \frac{1}{100 \omega_g^2 C_f} \quad (13)$$

Total harmonic distortion (THD) ratio of the RMS value of the harmonics to the RMS value of the fundamental and is defined as:

$$THD_i = \frac{\sqrt{\sum_{i=2}^n X_n^2}}{X_1} \quad (14)$$

where,

x_n is the r.m.s. of the harmonic voltage or current of the order n

X_1 is the r.m.s. of the fundamental voltage or current

3.2.2. Modeling of VSI

Voltage source inverter (VSI) is used to convert the DC PV power into AC power that is injected to the UG. The DC-AC power conversion process is carried out with the aid of a three-level voltage source inverter (3L-VSI). The advantages of such inverters are for [11, 12], improving voltage quality [13], reducing conduction loss and switching frequency, lowering blocking voltage and voltage tresses (dv/dt) on power switches. The simplified schematic diagram of a single leg of a three-level capacitor clamped VSI is shown in Fig. 7.

Table 5 lists the output voltage levels for one phase of the inverter. The state condition 1 means the switch is ON, and 0 means the switch is OFF.

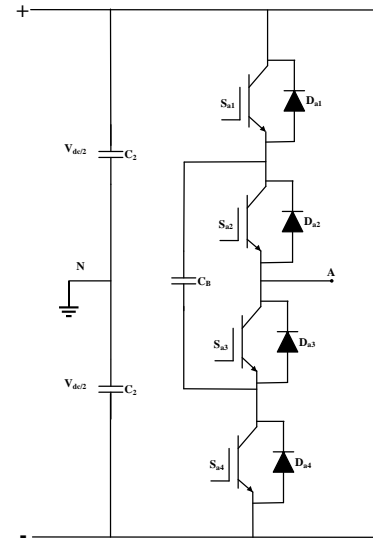


Fig. 7. Simple single leg of a three-level VSI.

SWITCHING STATES OF 3L-VSI

Pole voltage, V_{a0}	Switch State			
	S_{a1}	S_{a2}	S_{a3}	S_{a4}
Vdc/2	1	1	0	0
0	0	1	1	0
Vdc/2	0	0	1	1

3.2.3. MPPT control system

The MPPT controller uses the P&O MPPT algorithm of the PV panel voltage and current. Figure 8 illustrates the flowchart of the MPPT P&O modified algorithm [14, 15]. The flowchart shows that, at each sampling period, the MPP can be tracked by comparing the change in power, voltage and load demand with respect to zero to get the correct direction for perturbing the PV array voltage, V_{PV} to locate the MPP quickly where V_{PV} , equals to V_{mpp} at MPP. Once the MPP is reached, the operation of the PV array is maintained at this point unless there is change in ΔP , which indicates a change in solar radiation or weather condition. The algorithm decreases or increases V_{PV} to track the new MPP [14, 15]. This method provides better tracking of the MPP under fast-changing atmospheric conditions as compared with the conventional P&O method.

3.3. Control of Grid-Connected Inverter

Figure 9 shows the control scheme of VSI. A PLL is used to synchronize the inverter with the grid, where it takes the grid voltage and gives the frequency and phase angle of the grid voltage correctly even with distortion in the grid voltage [16]. The system control is composed of voltage and current regulators to improve the power factor and satisfy the synchronization requirements of the inverter with the UG in the synchronous frame. The Voltage Regulator minimizes variation in the DC voltage due to the change of the weather conditions via the PI controller. Voltage regulator generates command current I_d^* to process of its current regulator through comparing the measured DC voltage with setting DC voltage V_{dc}^* . The current regulator consists of PI controllers for both i_d and i_q currents. The command current I_d^* is drawn from Voltage regulator and compared with the grid current I_d .

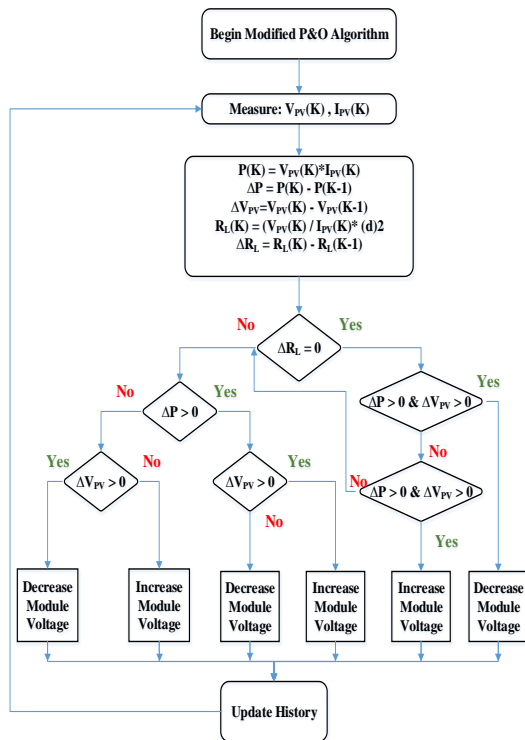


Fig.8. Flowchart of the P&O MPPT algorithm.

The compared signal (ΔI_d) is processed through the PI controller for minimizing the

error and producing, adding signal with generated voltage measuring signal (V_d) to compare with ω_L to produce V_d^* command. Also, the command current I_q^* is equal to zero to improve the power factor of inverter up to unity. The signal (ΔI_q) is processed through the PI controller to produce adding signal with generated voltage (V_q) and ωL to produce V_q^* command. The outputs of the PI controllers are processed through the hysteresis band to limit the errors between upper and lower limits. The ($dq0$) is converted into the three-phase (abc) to PWM.

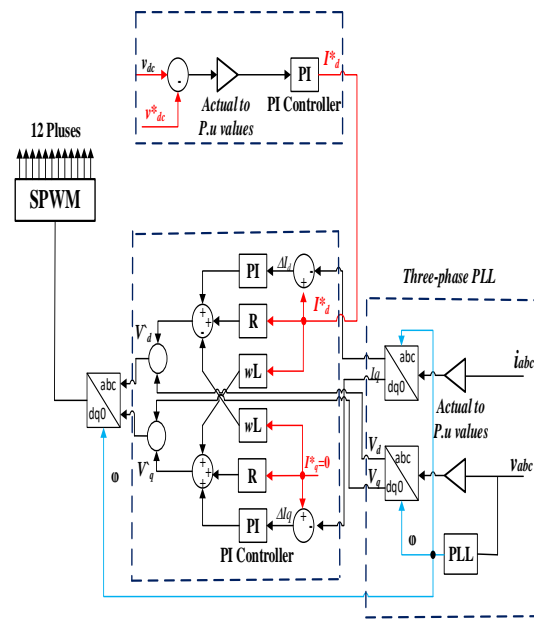


Fig.9. Control scheme for three-phase grid-connected VSI.

4. DISCUSSION AND RESULTS

4.1. Evaluated the recorded measurements of the SSPV according to Egyptian PV-LV code-2014

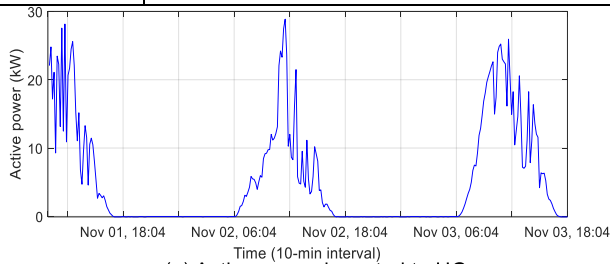
Power quality parameters are measured for the output of the installed PV system at the considered site by using PA-9 plus power quality analyzer at PCC. The power quality parameters recorded are the active power, voltage, reactive power, power factor, flicker and THD are measured as well over a period from 01/11/2016 at 10:14 to 03/11/2016 at 18:04. The power quality provided by the SSPV systems is governed by practices and standards according to the Egyptian PV-LV code.

Figure 10 (a) shows the active power injected to UG which has a fluctuating during sun hours (from sunrise to sunset).

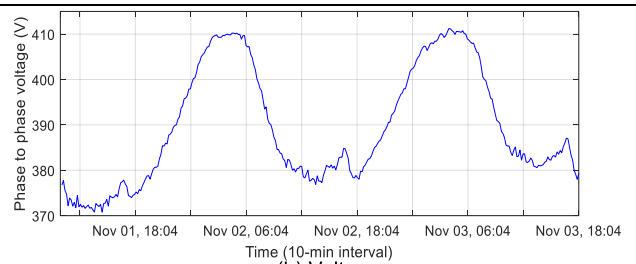
Table 6 evaluates the recorded measurements according to the Egyptian PV-LV code.

TECHNICAL REQUIREMENTS OF SSPV BASED ON EGYPTIAN PV-LV CODE-2014

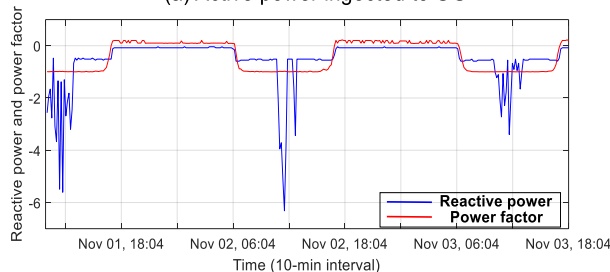
System Parameter	Egyptian PV-LV Code-2014 (<500kW)	Evaluated the Recorded Measurements according to Egyptian PV-LV code
Voltage operation range	shall operate within the limits of the voltage variation in the range of $\pm 10\%$ of the nominal voltage	Figure 10(b) shows the voltage variation operates within the limit in the range of 413V (+8.7%) to 471V (-2.4%) and passes according to PV-LV code.
Power factor operation range	shall be limited to a power factor of 0.9.	Figure 10(c) shows the reactive power fluctuation follow the active power fluctuation to achieve PF which nears to unity at sun hours and passes according to PV-LV code. This is due to the integrated control of the reactive power in the used inverter. Where modern intelligent inverter designs are now beginning to consider the issue of the reactive power control by providing better compensation based on system parameters and the needs of the distribution networks.
Frequency operation range	shall operate within the frequency trip limits (48.5 Hz ~ 51 Hz)	Figure 10(d) shows the frequency fluctuation operates within the limit in the range of (49.9 – 50.4 HZ) and passes according to PV-LV code.
Flicker	<ul style="list-style-type: none"> ▪ The short-term flicker severity (P_{st}) is 1. ▪ The short period for measuring is 10 minutes. 	Figure 11(a, b) show P_{st} doesn't exceed 0.7 and P_{lt} doesn't exceed 0.5 and operate within the limit of operation range according to PV-LV code.
	<ul style="list-style-type: none"> ▪ the long-term flicker severity (P_{lt}) is 0.8. ▪ long period for measuring is 2 hours. 	
THD	Total harmonic distortion shall be less than 5 % at rated generator output in accordance with IEC 61727:2004.	<ul style="list-style-type: none"> ▪ Figure 11(c) shows the voltage THD < .035 % and passes according to PV-LV code. ▪ Figure 11(d) shows the current THD doesn't exceed 5% at sun hours and passes according to PV-LV code.



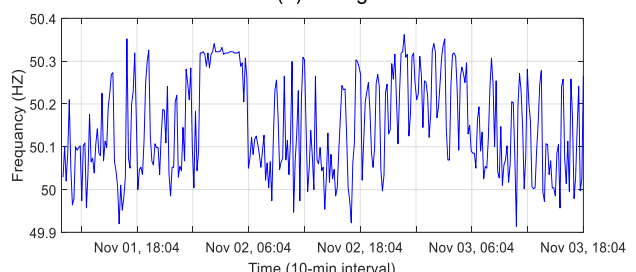
(a) Active power injected to UG



(b) Voltage



(c) Reactive power (kVar) and power factor



(d) Frequency

Fig.10. The active power, voltage, power factor, frequency records (Measurements).

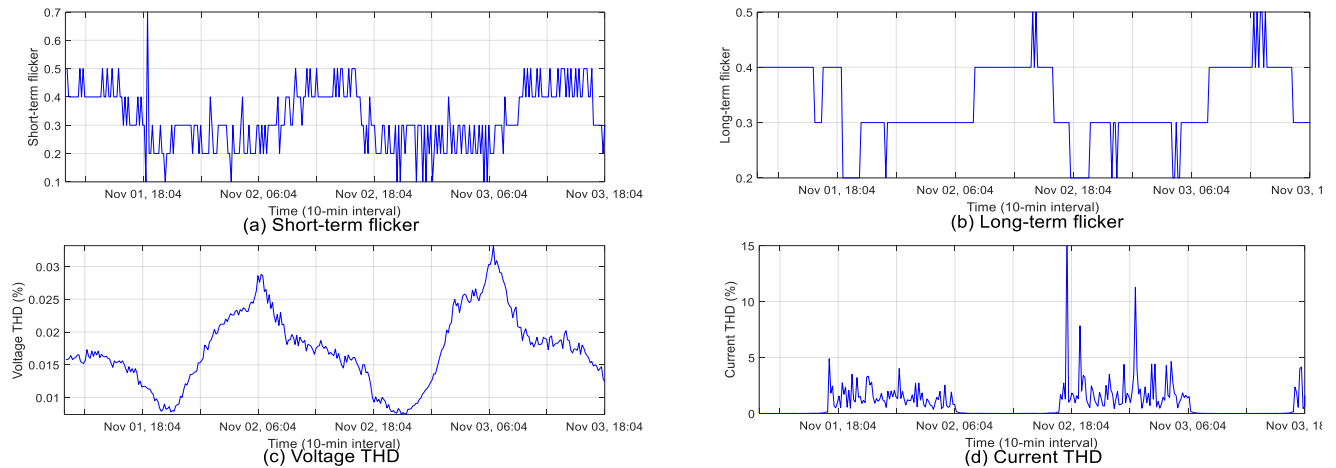


Fig.11.The flicker and THD (Measurements).

4.2. Performance analysis of SSPV power quality based on Simulation

To investigate the various effects for connecting SSPV system to LV distribution networks simulated 39.78 kW grid-connected PV system (likewise the real case) by MATLAB SIMULINK and measured PV system output parameters.

There are two cases, one with varying assumed solar irradiance values (fluctuating between 1000~500 W/m²) and the other with actual solar irradiance that are obtained from statistics. The temperature is assumed constant (25 °C) in the two cases.

Case 1: This case is designed to compute the performance under variable solar irradiance ranging between 1000 W/m² and 500 W/m². A Simulink model is employed to estimate the effects of changing irradiance on a PV system.

Figure 12(a) shows the hypothetical solar radiation distribution over the day that categorized to sunrise, sunny, thin low start cloud, and sunset period. Figure 12(b, c, d) shows PV Side results. Figure 12(b) shows the PV array output power starts to appear as the radiation increased at 06:00 a.m. and reaches to a steady-state value of 37.75 kW when the radiation becomes 1000 W/m² at 8:00 a.m. After applying the MPPT algorithm at 9:50 the output power increased by about 4.84 % to be 39.67 kW. A low percentage of power increased due to MPPT as the duty cycle is adjusted to a value ($D = 0.5$) that gives the DC link voltage level

directly. When the radiation decreased to 800 w/m² during (10:15 to 12:00 a.m.) due to thin low stratus clouds, the output power also decreased to 32 kW. If the radiation is further decreased to 500 w/m² during (14:00 to 15:00 p.m.) due to larger clouds, the output power also decreased to 17.5 kW. Figure 12(c) shows the simulated PV array voltage and current during the hypothetical solar radiation distribution. From this figure, the output voltage is still constant and PV current also is linear with solar irradiance. Figure 12(d) shows the duty cycle with and without applying algorithm MPPT which provides substantially more power as shown in Figs. 12(b) and 13(a).

Figure 13 shows grid side results. Figure 13(a, b) shows that the active power which is injected into the grid, is linearly varied with the solar irradiance but the reactive power follows the active power to achieve the unity power factor. Figure 13(c) shows the simulated voltage and current waveforms of phase A before the transformer. From this figure, the voltage and current injected to the grid from the PV system at the PCC are in phase (unity power factor). Figure 13(d) shows the output voltage and zoom version of 3L-VSI before and after LC filter which reduces ripple content at the output.

Figures 14 and 15 show the voltage and current THD. The IEEE standard for THD is less than 5%. THDs below 5% are widely considered to be acceptable, while values above 10% are unacceptable and will cause problems for sensitive equipment and loads. Figure 14 shows the voltage THD before and

after the filter. It is noted that the installation of LC filter reduces the amount of THD from 89.13% to 0.8%. Figure 15 shows the current THD versus harmonic order, simulated time and solar irradiance. From this figure, the

current THD decreases significantly at high solar irradiance conditions and increases at low solar irradiance. Current THD very sensitive to changes in incident radiation.

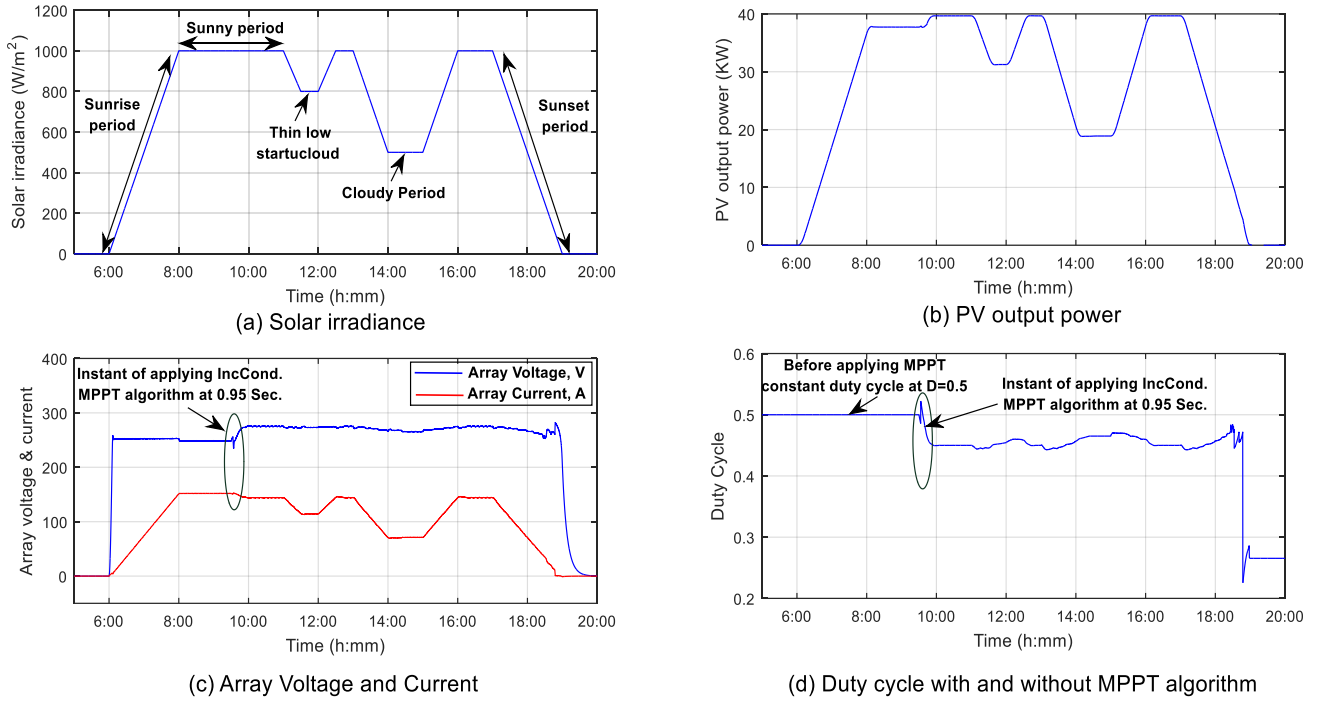


Fig.12. The assumed solar irradiance and PV side results.

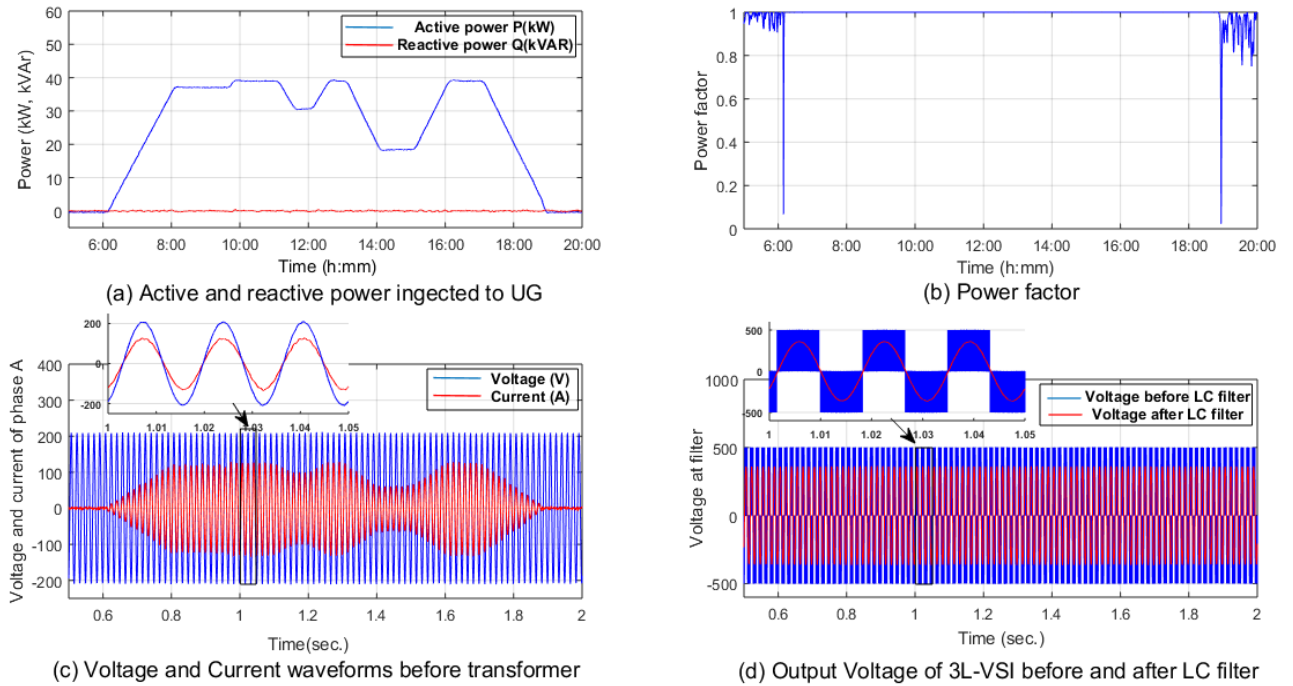


Fig. 13. AC Side results for assumed irradiance.

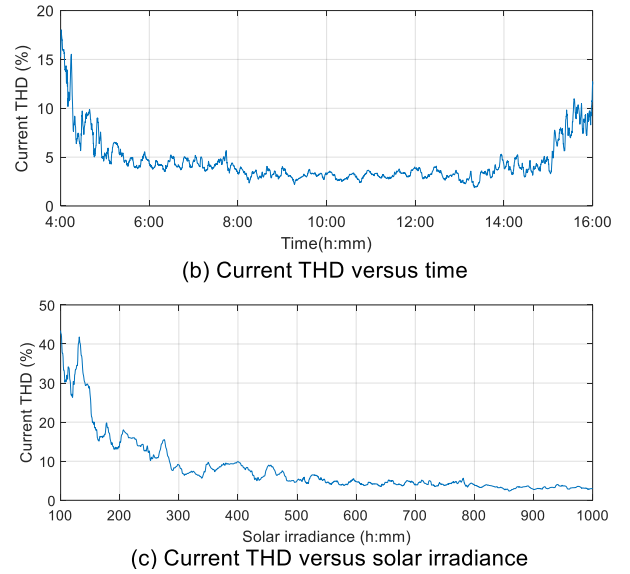
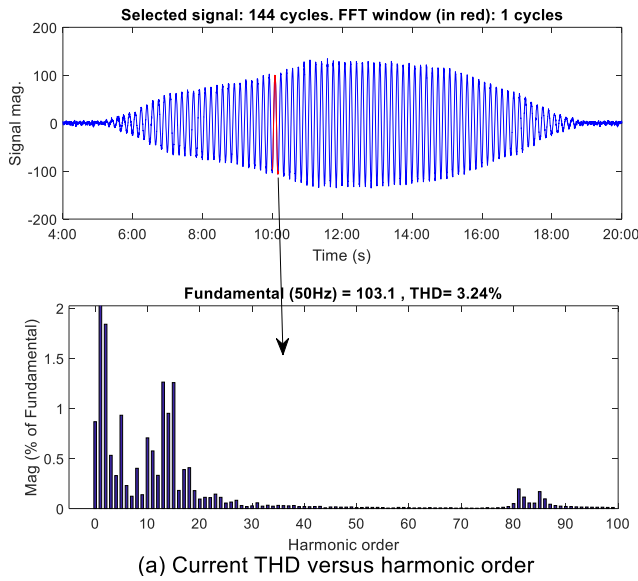


Fig. 14. Voltage THD before and after LC filter.

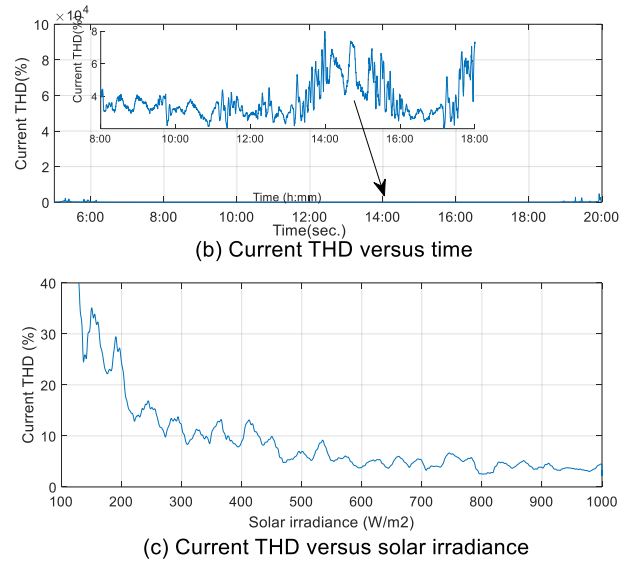
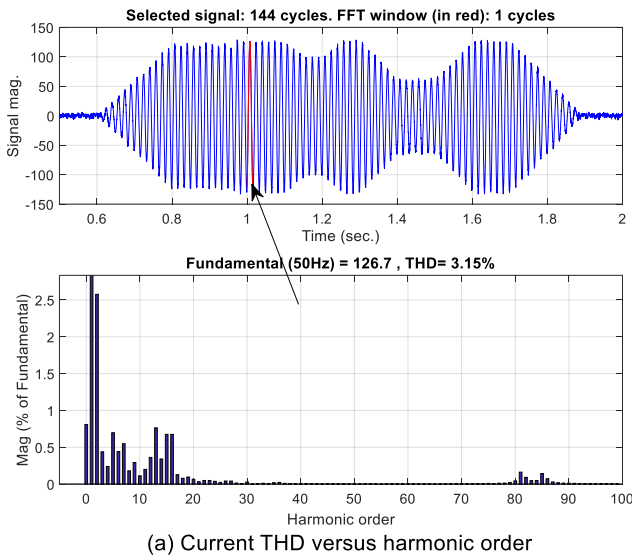


Fig. 15. The current THD.

Case 2: the second examined case is for actual solar irradiance for a day as shown in fig. 16(a).

Table 7 lists the simulation results and discusses PV sides results, grid side results, voltage THD and current THD as shown in Fig. 16, 17, 18 and 19 respectively.

SIMULATION RESULTS OF CASE 2

<i>Parameters</i>	<i>Discuss Simulation results of case 2</i>
PV side results	<ul style="list-style-type: none"> ▪ Figure 16 (b) shows the PV output array is strongly dependent on solar irradiance fluctuation. ▪ Figure 16(c) shows the voltage and current array. From this figure, the PV current is strongly dependent on solar irradiance, but the PV voltage is constant with irradiance variation. ▪ Figure 16(d) shows the actual voltage fluctuates to follow the reference voltage of MPPT algorithm.
Active Power	<ul style="list-style-type: none"> ▪ Figure 17(a) shows The active power produced by the system is strongly dependent on solar irradiance fluctuation. ▪ Fluctuations of solar irradiance lead to fluctuations of active power supplied to the distribution network. ▪ when solar irradiance is low, the produced active power of PV unit is low. ▪ The active power delivered to the distribution network is found to vary linearly with the fluctuation of the solar irradiance incident on the PV modules
Reactive Power and power factor	<ul style="list-style-type: none"> ▪ Figure 17(a) shows the reactive power is dependent on the active power of the inverter for maintaining the power factor to the accepted levels as shown in Fig. 17(b) which in turn is affected by solar irradiance levels. This is due to the integrated control of the reactive power in the used inverter. Where modern intelligent inverter designs are now beginning to consider the issue of the reactive power control by providing better compensation based on system parameters and the needs of the distribution networks. ▪ The results of the power factor are found to be acceptable for a large fraction of the day, but it can also be observed that the power factor falls below the acceptable limits during the time of low solar irradiance. ▪ The power factor is shown to act linearly for values of solar irradiance lower than 200 W/m² while stays close to unity for the higher values.
Voltage THD	<ul style="list-style-type: none"> ▪ A major power quality problem in power electronic converter applications results from the voltage/current THD provided by the inverters. ▪ Figure 18(a) shows the voltage THD doesn't exceed 1.4%. ▪ Figure 18(c) and 18(d) show the voltage THD versus harmonic order before and after LC filter. From these figures, it can be observed that the installation of LC filter reduces the amount of THD for 3L-VSI topologies from 90.86% to 0.96%. ▪ The harmonics generated by the inverter are reduced through the passive filter.
Current THD	<ul style="list-style-type: none"> ▪ the current THD versus harmonic order is shown in fig. 19(a). ▪ the current THD increases significantly at low solar irradiance conditions in sunrise and sunset as shown in Fig.19(b). ▪ the current harmonics (fig. 19(c)) are very sensitive to changes in incident radiation. These results confirm that the high harmonic content has occurred at the low solar radiation values.

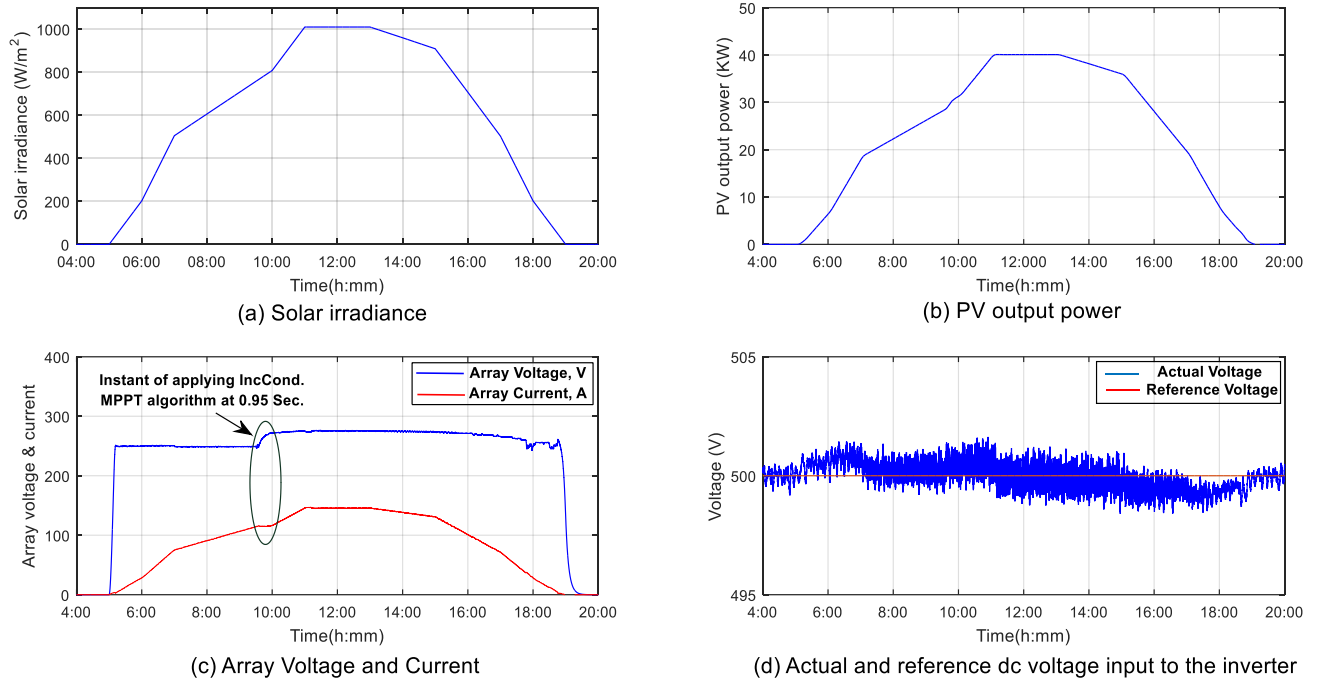


Fig. 16. Actual irradiance and PV side results.

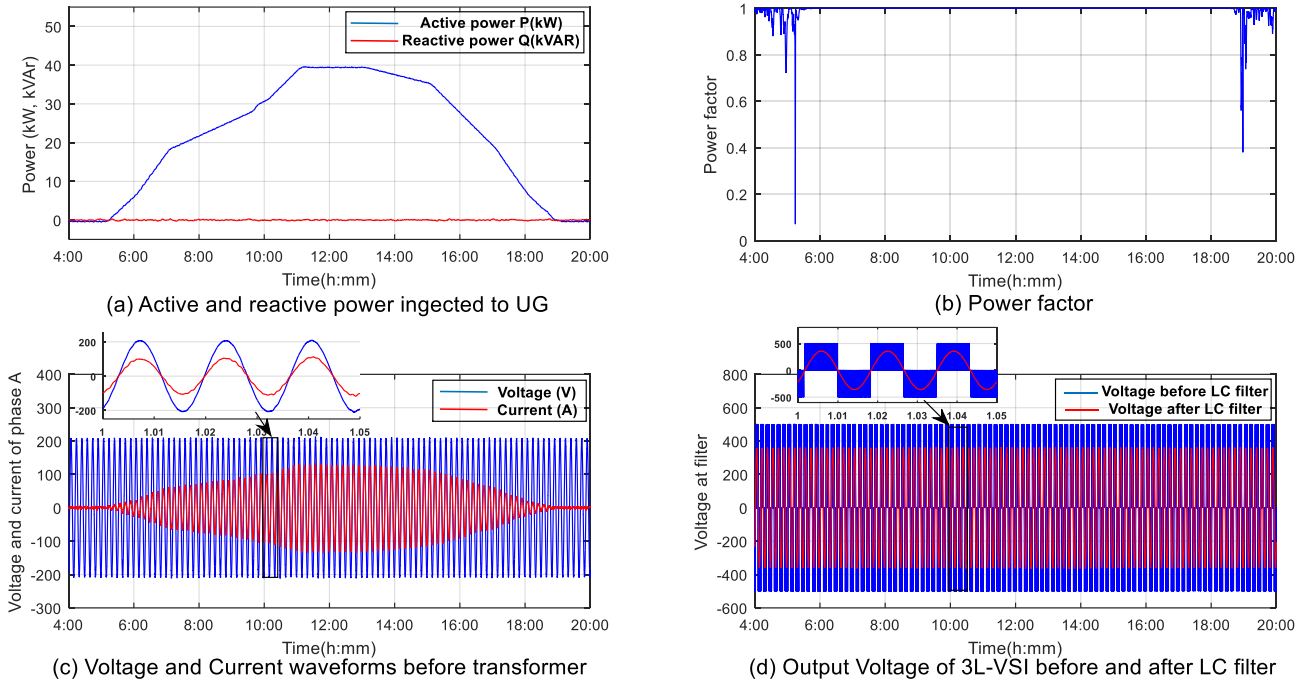


Fig. 17. Grid side results for actual irradiance.

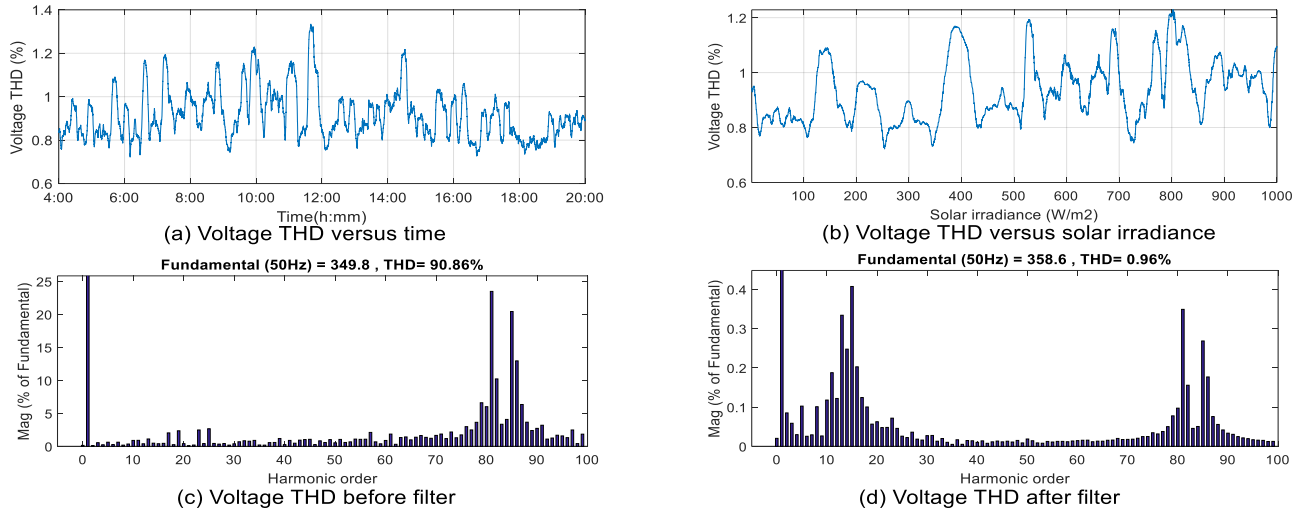


Fig. 18. Voltage THD before and after LC filter for actual irradiance.

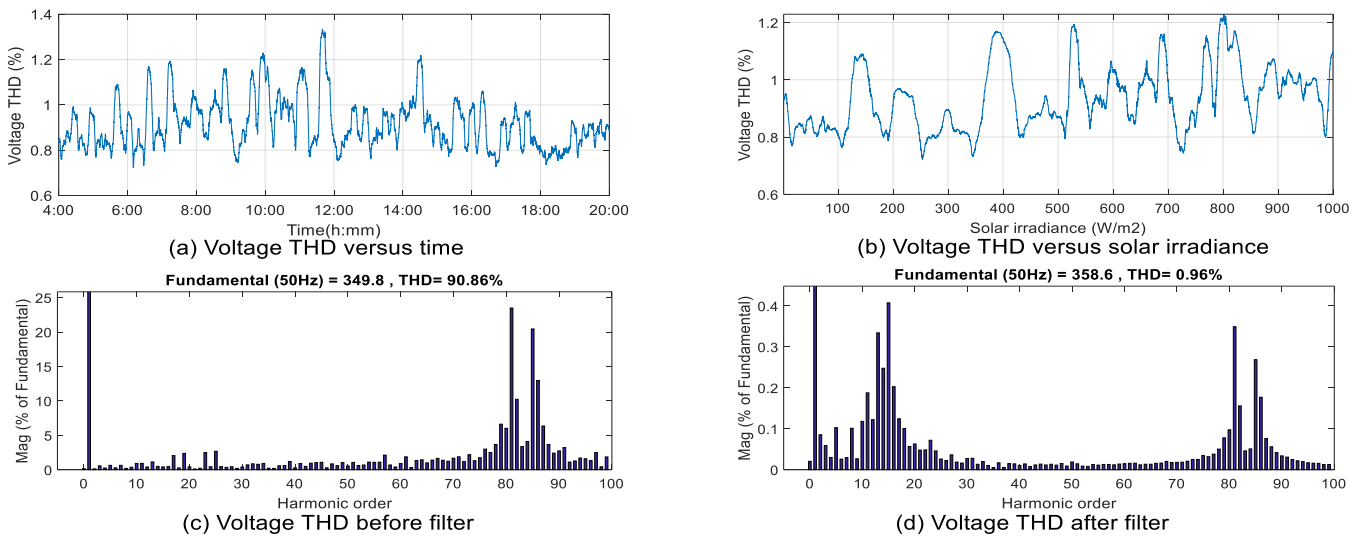


Fig. 19. Current THD for actual irradiance.

4.3. Cost analysis:

Although their installation costs are high at the beginning, PV generators are cost-effective in terms of operation and maintenance. The systems become more and more efficient thanks to technological developments, and costs are gradually reduced.

Figure 20 was exported from the sunny design [12] which shows the energy yield per month and the annual energy yield of the designed PV power plants. From the figure, the annual energy yield equals to 68.627MWh. The cost analysis of a 39.78 kW grid-connected PV power plant is given in Table 8. Figure 21 shows yearly financial

balance and payback of the considered system.

The considered system installed in October 2016 to provide energy for a textile factory generates 68.627 MWh of energy and reaches its initial cost in 6.1 years. This significant renewable energy source bears the utmost importance in today's world where the need for and cost of energy is considerably high. In addition to its cost-efficiency, the system is also environmentally friendly. It does not lead to gas emission or contribute to global warming. It is observed that PV generators are significantly useful when climatic conditions are considered.

COST ANALYSIS OF 39.78 kW GRID CONNECTED PV SYSTEM

PV Panels	STP255-20/wd	156 PCS	6.2 EGP/W att	246,636 EGP
Support	Aluminum	156 PCS	1200 EGP/K W	47,736 EGP
Inverter	STP 20000TL-30	2 PCS	24,000 EGP/P CS	48,000 EGP
Cable	AC	CX1-4×16 mm²	100 m	120 EGP/m
	DC	KPE 6mm²	1,000 m	8 EGP/m
Protection	AC protection	SET	1,000 EGP	1,000 EGP
	DC protection	SET	1,500 EGP	1,500 EGP
	Earthing	SET	10,000 EGP	10,000 EGP
Installation		39.78 kW	350 EGP/k W	13,923 EGP
Total		377,995 EGP		
Taxes		10 %	37,799.5 EGP	
Net investment	415,794.5 EGP			
System Costs (EGP/W)	10.45 EGP/W			
Fixed feeding tariff	1.08 EGP			
Annual energy yield	68,627 kWh			
Total yearly income	74,117 EGP			
Total income (25 years)	1,852,929			
Maintenance cost (1 year)	6,000 EGP			
Net profit	1,702,929 EGP			

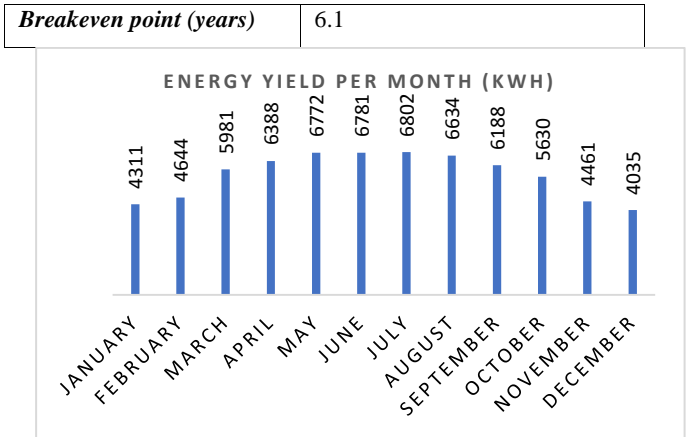


Fig. 20. Energy yield per month.

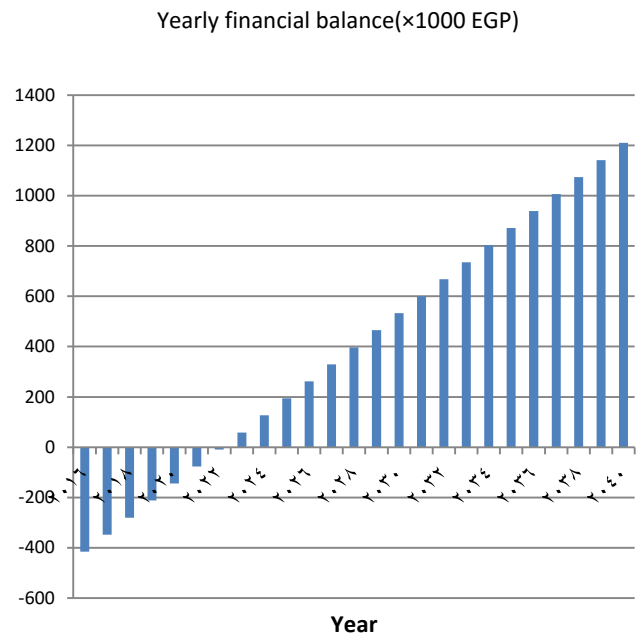


Fig. 21. Yearly financial balance.

5. CONCLUSION

The power quality observations of the PV grid-connected system which is installed in Egypt have been presented. A 39.78 kWp grid-connected PV system was simulated using Matlab/Simulink software under different solar irradiances. Measurements from the PV array under test have been analyzed and evaluated to observe the overall effect of technical requirements according to the Egyptian PV LV code of the PV grid-connected system under test and cost analysis. It has been found that a low solar irradiance has a significant impact on the power quality of the output of the PV system. The results show that the active power produced by the PV system causes a voltage rise, voltage flicker, and power factor reduction, which may create severe problems with the system components. The system installed in October 2016 and able to provide the energy for a textile factory and also the system generates 68.288 MWh of energy and reaches its initial cost in 6.137years.

REFERENCES

- [1] Bae, Y., T.-K. Vu, and R.-Y.J.I.T.o.E.C. Kim Implemental control strategy for grid stabilization of grid-connected PV system based on German grid code in symmetrical low-to-medium voltage network. 2013. 28(3): p. 619-631.
- [2] E Caamaño-Martín, H. Laukamp et al., Interaction between photovoltaic distributed generation and electricity networks. *Progress in Photovoltaics: research and applications*, 2008. 16(7): p. 629-643.
- [3] El kholy, A., et al., Experimental evaluation of 8kW grid-connected photovoltaic system in Egypt. *Journal of Electrical Systems and Information Technology*. 3(2): p. 217-229.
- [4] Micheli, D., et al., Analysis of the outdoor performance and efficiency of two grid connected photovoltaic systems in northern Italy. 2014. 80: p. 436-445.
- [5] Kageyama, H., et al. Measurement of inrush-current waveforms for modeling reactance characteristics of pv modules. in 26th European Photovoltaic Solar Energy Conference and Exhibition. 2011.
- [6] Sharma, S. and B. Parekh. Impact of pvps (photovoltaic power system) connection to grid in urban areas. in National Conference on Recent Trends in Engineering & Technology. 2011.
- [7] Wang, B., et al. Dynamic modeling and transient fault analysis of feeder in distribution system with MW PV substation. in Universities Power Engineering Conference (UPEC), 2010 45th International. 2010. IEEE.
- [8] Farhoodnea, M., et al., Power quality analysis of grid-connected photovoltaic systems in distribution networks. *Przegląd Elektrotechniczny (Electrical Review)*, ISSN 0033-2097, 2013. 89(2), 2013: p. 208-213.
- [9] Farhoodnea, M., et al., An enhanced method for contribution assessment of utility and customer harmonic distortions in radial and weakly meshed distribution systems. *International Journal of Electrical Power & Energy Systems*, 2012. 43(1): p. 222-229.
- [10] Hassan, M. Performance Analysis of Grid-Connected PV System. in 18th International Middle-East Power System Conference (MEPCON'16), Helwan, Egypt, December 27-29. 2016.
- [11] Halpin, S. Revisions to iee standard 519-1992. in IEEE PES transmission and distribution conference and exhibition. 2006.
- [12] <https://www.sunnydesignweb.com/sdweb/#/> Home, Access 21 November 2019.

تحليل أداء نظام الطاقة الشمسية المتصل بالشبكة: دراسة حالة في مصر

المخلص:

أصبحت مصادر الطاقة المتجددة ، وخاصة الأنظمة الكهروضوئية ، مصادر أكثر أهمية للطاقة ، مما جذب اهتمام تجاري كبير. ومع ذلك ، فإن توصيل أنظمة الطاقة الكهروضوئية بشبكات القوى الكهربائية الموحدة قد يسبب العديد من المشكلات لشبكات التوزيع عند التشغيل. تعتمد شدة هذه المشكلات بشكل مباشر على النسبة المئوية للقوى الكهربائية المولدة من خلايا الطاقة الشمسية والموصلة الى الشبكة وايضا جغرافيا التثبيت. وبالتالي ، فإن معرفة التأثير المحتمل للأنظمة الكهروضوئية الصغيرة المتصلة بالشبكة على شبكات التوزيع يمكن أن توفر حلولاً ممكنة قبل التطبيقات العملية. تعتمد الطاقة الكهربائية المولدة من محطات الطاقة الشمسية (PV) بشكل رئيسي على الظروف المناخية. لذلك ، يجب أن تزود هذه المحطات المتصلة بالشبكة بنظام التحكم لتلبية استجابة سريعة لتغيير الإشعاع الشمسي. تتضمن هذه الدراسة تحليل أداء للبيانات والقياسات الفعلية من موقع النظام المتصل بالشبكة وفقاً للكود المصري PV-LV لعام ٢٠١٤ ، والمحاكاة باستخدام برنامج المحاكاة MATLAB / Simulink ، وايضا تحليل التكلفة لربط الخلايا الكهروضوئية الصغيرة الحجم في حدود ٣٩.٧٨ كيلو واط بشبكات التوزيع. وايضا يتم قياس مؤشرات جودة الطاقة من محطة الطاقة الشمسية المثبتة في مدرسة Holy Family

School في مدينة حلوان ، مصر.

اليف اللب من ٠.١ % إلى ٠.٤ %.